Department of Pharmaceutics[1], Institute of Pharmacy, Biopharmaceutics & NutriCosmetics, Freie Universität Berlin, Germany, C.U. Shah College of Pharmacy[2], S.N.D.T. Women's University, Santacruz West, Mumbai, India

Stavudine entrapped lipid nanoparticles for targeting lymphatic HIV reservoirs

R. Shegokar[1,2], K. K. Singh[2]

Received May 19, 2010, accepted August 2, 2010

Dr. K.K. Singh, Professor of Pharmaceutics, C.U. Shah College of Pharmacy, S.N.D.T. Women's University, Santacruz West, Mumbai, India
kksingh35@rediffmail.com

Pharmazie 66: 264–271 (2011) *doi: 10.1691/ph.2011.0149*

The main objective of present research study was to evaluate the potential of lipid nanoparticles for active delivery of an antiretroviral drug to lymphatic tissues. Stavudine entrapped drug loaded solid lipid nanoparticles (SLNs) were prepared and characterized for a variety of physicochemical parameters such as appearance, particle size, polydispersity index and zeta potential. The targeting potential of the prepared nanoparticles was investigated by carrying out *ex vivo* cellular uptake studies in macrophages which depicted several times enhanced uptake as compared to pure drug solution. Further, the lymphatic drug levels and organ distribution studies demonstrated efficiency of the developed nanoparticles for prolonged residence in spleenic tissues. Thus it was concluded that stavudine entrapped lipid carriers can be exploited for effective and targeted delivery to cellular and anatomical HIV reservoirs and may ultimately increase the therapeutic safety and reduce side effects.

1. Introduction

Acquired Immunodeficiency Syndrome (AIDS) is one of the most frightening syndrome worldwide. Cellular HIV reservoirs include memory CD4+T lymphocytes, blood monocytes and macrophages/cells. Anatomical reservoirs of HIV occur in tissues that are immunologically sheltered or separated by a barrier from the blood and lymphoid systems and include mainly CNS, lymphatic system especially lymph nodes, testes, intestinal, vaginal epithelium, kidney, liver, eye and lungs. These reservoirs are characterized by their stability, and are believed to act as sanctuaries from the effects of drugs and host immune responses during HAART (Lanao et al. 2007) significantly contributing to viral persistence. Direct infiltration of the HIV in these reservoir sites makes AIDS treatment extremely difficult, as many drugs cannot adequately reach or reside in these sites in sufficient concentrations and for the necessary duration to exert the therapeutic response (Vyas et al. 2006a). As penetration of antiretroviral (ARV) drugs into the viral reservoir sites is restricted, a high dose has to be given with consequent intolerance (Amiji et al. 2006) and toxicity. In addition many drugs can't adequately reach or reside in these sites in sufficient concentrations and for the necessary duration to exert the therapeutic response (Vyas et al. 2006b).

Several studies involving ARV drug loaded nanoparticles for targeting to the macrophages have consequently emerged. Schafer et al. (1992) prepared AZT loaded polyalkylcyanoacrylate (PACA), poly methyl methacrylate (PMMA) and human serum albumin (HSA) nanoparticles which showed enhanced uptake into HIV infected macrophages and confirmed potential of AZT and ddC human serum albumin nanoparticles for the targeting of macrophages. Löbenberg et al. (1998) investigated the oral delivery of AZT – hexylcyanoacrylate nanoparticles for delivery to the reticulo-endothelial cells in rats and observed that AUC of radiolabelled AZT in the liver was 30% higher for nanoparticles than that of drug solution and also higher drug levels in blood and brain as compared to the control solution. The same formulation when tested after intravenous administration led to AZT concentrations up to 18 times higher in organs of the RES as compared to pure drug solution (Löbenberg et al. 1998). Kuo (2005) effectively developed stavudine loaded polybutylcyanoacrylate (PBCA) and methylmethacrylate sulfo- propylmethacrylate (MMA-SPM) nanoparticles for brain targeting. More recently, Dou et al. (2007) proposed that the mononuclear phagocytes, as the principal reservoir for viral dissemination, could serve as a transporter of antiretroviral drugs themselves, i.e. macrophages can enter tissues that limit entry of many ARV drugs. They have described a macrophage-based nanoparticulate system as a carrier itself for indinavir (INV), a nanoparticle indinavir (NP-INV) formulation packaged into bone marrow derived macrophages (BMMs). The effects of this drug carrier on biodistribution and disease outcomes were assessed in immune competent and human immunodeficiency virus type 1 (HIV-1) infected humanised immune-deficient mice (Dou et al. 2006). Significant lung, liver and spleen BMMs and drug distribution were observed. The use of ligands on nanoparticles for receptor-mediated targeting has been reported in the literature. So Jain et al. (2008) developed mannosylated gelatine nanoparticles (MN-G-NP) (248–325 nm). *Ex vivo* studies using alveolar macrophages from rats showed 18.0 and 2.7 times higher uptake by the macrophages from MN-G-NPs as compared to uncoated G-NPs respectively.

Nanoparticles (10–1000 nm) made from solid lipids are attracting increasing attention as colloidal drug carriers for various

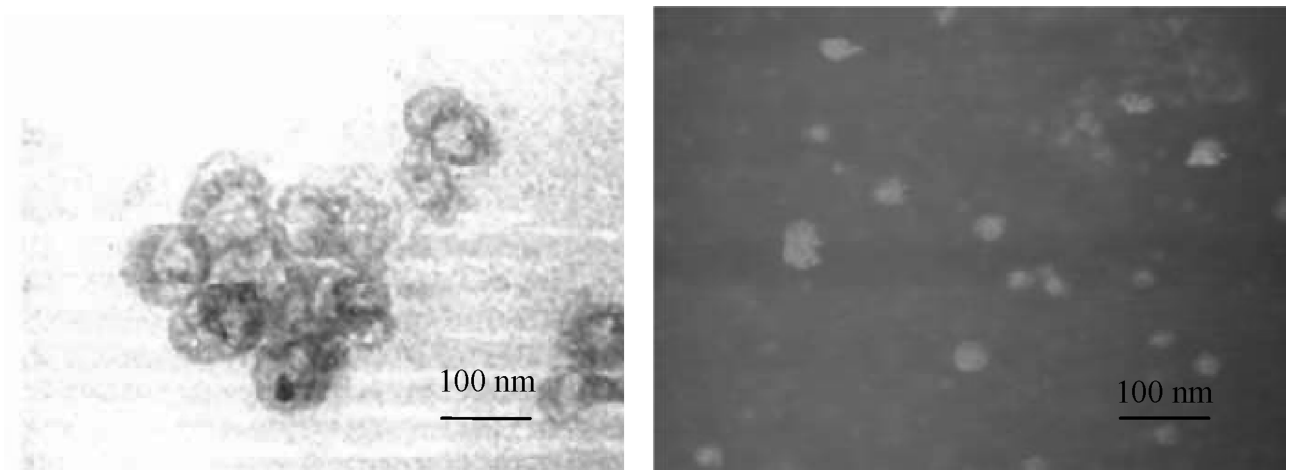

Fig. 1: TEM photomicrograph (left) and Atomic force microscopy images of stavudine lipid nanoparticles (right)

applications because of their biodegradable nature, non-toxicity and lower cost of ingredients (zur Mühlen et al. 1998). The interaction of lipid nanoparticles with cells and phygocytic uptake, the intracellular tolerability and degradation velocity are important parameters to assess the possible application. In the 1990s SLN were developed as an alternative colloidal carrier system for emulsions, liposomes and polymer nanoparticles in controlled drug delivery (Mehnert and Mäder 2001). As they are composed of physiological lipids they are easily taken up by cells. Compared with other colloidal carriers, lipid nanocarriers have unparalleled advantages including the ability to entrap material with different solubilities, the scalability possibility using natural ingredients on industrial scale, biocompatibility and targetability (Hou et al. 2003).

Stavudine is a Nucleoside Reverse Transcriptase Inhibitor (NRTIs), active against zidovudine and didanosine resistant strains. It is intacellularly phosphorylaterd to an active metabolite, stavudine 5'-triphosphate. This metabolite inhibits HIV replication, either by competing with thymidine 5'-triphosphate for incorporation into viral DNA by reverse transcriptase or by causing premature termination of the viral chain after incorporation. The stavudine triphosphate even interferes with the DNA beta and gamma polymerase (Guimaraes et al 2010). It is currently approved by US FDA to patient resistant to zidovudine, didanosine or zalcitabine therapy (Escobar et al. 2003). Long term administration of stavudine over a period results in various adverse effects such as a dose limiting peripheral neuropathy and potentially limiting side effects including anemia, insomnia and malaise. A nanoparticulate drug carrier can alleviate drug toxicity and also deliver the drug directly to the target site in a passive manner reducing adverse side effects.

In this study we report the development and characterization of lipid nanoparticles of stavudine with robust particle size control, stability and superior targeting of antiretroviral drug molecules (Sosnik et al. 2009). The blood clearance, lymph kinetic, gamma imaging and biodistribution for radiolabelled pure drug, blank and drug loaded nanoparticles were carried out in rats. The prepared lipid nanoparticles showed enhanced levels in major HIV reservoir sites in body. Macrophage uptake study revealed the potential of the lipid nanoparticles prepared for targeting intracellular compartments and eradication of viral load from the cellular and anatomical reservoir sites focusing on the future outlook to treat HIV/AIDS.

2. Investigations, results and discussion

2.1. Preparation and optimization of nanoparticles

Trimyristin showed good solubility for stavudine which could be further enhanced by addition of surfactants. Combination of hydrophobic surfactants was found to stabilize the system more effectively than a single surfactant system. The lipid nanodispersions were subjected to homogenization pressures in the range of 200–800 bar keeping a number of homogenization cycles constant i.e., two. Particle size of trimyristin nanodispersions increased at higher homogenization pressure i.e., at 600 to 800 bars to 104 nm. Increase in particle size can also be attributed to aggregation of the particles resulting from higher temperature built during homogenization at higher pressure. The additional energy input let to higher kinetic energy of the droplets with subsequent coalescence. The lowest mean particle size of 75 nm was obtained at 200 bar pressure and 2 cycles. The surfactants played a very important role in determining particle size. The rate of addition of lipid phase to water phase dramatically affected the particle size.

2.2. Characterization of nanoparticles

The stavudine lipid nanoparticles were odourless bluish transparent to white colored translucent dispersions. No sign of instability was observed. The pH of the lipid of nanodispersion was 7.08 ± 0.11. Nanoparticles were stable even at high centrifugal force. Drug content of prepared nanoparticles of stavudine was determined and found to be $96 \pm 4.42\%$.

Particle size analysis showed a mean particle size of 75 ± 1.22 nm with a narrow particle size distribution below 300 nm. The lower polydispersity index of 0.120 confirmed the narrow particle size distribution. LD particle size range data revealed that more than 90.0% particles were smaller than 200 nm (d(v)90%). The d(v)95% and d(v)99% was below 180 nm and 220 nm, respectively. Results obtained with photon correlation spectroscopy and laser diffractometry were comparable.

Zeta potential measured in distilled water was close to the stern potential which is related to the potential of the particle surface (Nernst potential). The higher is Nernst potential is the higher is stern potential and related high zeta potential promoting stability to the particle. The zeta potential in miliQ water was observed to be -34.48 mV confirming the stability of system.

The transmission electron micrograph of the nanodispersion confirmed the spherical shape and narrow size distribution of the particles. It was observed that the particles were smaller that 200 nm (Fig. 1). Thus the formulated nanodispersions have the desired particle size distribution.

Differential Scanning Calorimetry (DSC) one of the most widely used calorimetric technique for qualitative and quantitative determinations of physiochemical properties of a drug. Fig. 2 presents the DSC thermographs of lipid nanoparticles. Melting

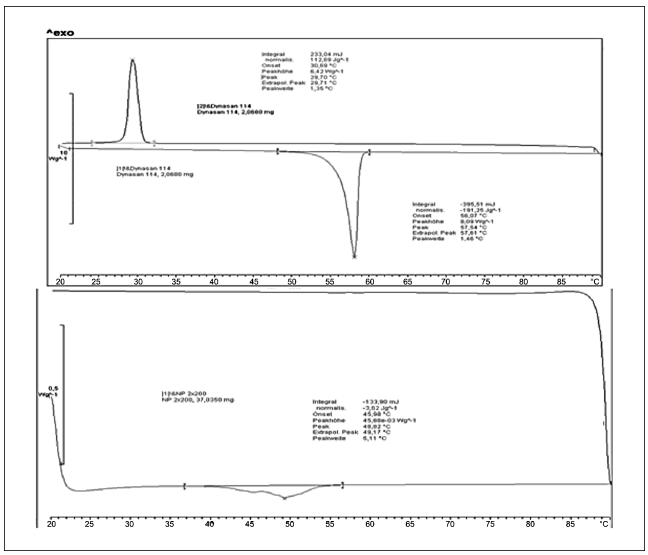

Fig. 2: Differential scanning thermograms of pure lipid (above) and lipid nanoparticles (below)

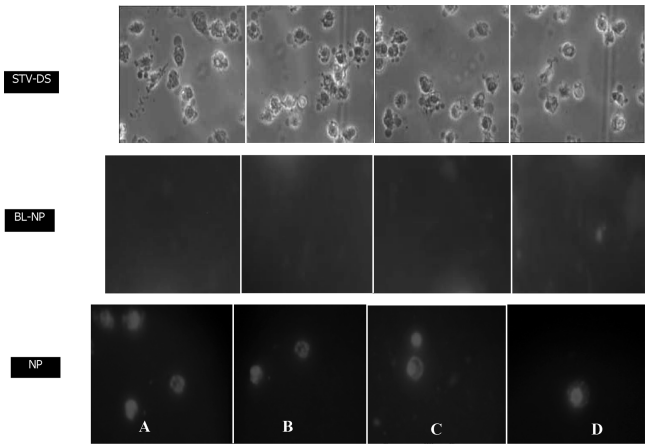

Fig. 3: Fluorescence photomicrographs of primary macrophages incubated with fluorescently labeled nanoparticles A) 10 min B) 30 min C) 60 min and D) 120 min

point depression was observed after drug entrapment and conversion into nanoparticles. In case of pure lipid the melting was around 58 °C. After homogenization the melting point was further suppressed to 48–49 °C. DSC studies revealed differences in the peak temperatures and melting enthalpies of lipid peak between pure lipid and drug incorporated nanoparticles.

Changes of more than two degrees in the peak temperatures are usually associated with new crystalline forms or entrapment of a new moiety. Since the thermodynamic behaviour of the small particles of nanometer size is different from than that of micronized ones, the DSC thermograms confirmed the rule that melting temperature of nanometer sized material will be much lower than that of bulk substance. Further surface modifications did not affect thermal behaviour very low of formulation, no additional peak was observed for the surface modifier probably due to the overall concentration of surface modifier in the formulation. Similar oberservations were made by Al-Haj and Rasedee (2009) during thermal analysis of solid lipid nanoparticles.

2.3. Cellular uptake studies

The cationic fluorochrome rhodamine 123 (R123), is mitochondria specific fluorescent probe in living cells without passage through endolytic vesicles and lysosomes. Fluorescence was not detected in control cells that had not been exposed to the fluorescent nanoparticles. Effect of incubation time on the cellular uptake is reflected by the quantitative measurement showing stronger fluorescence in the cells with the increase of incubation time from 0.5 to 2 h. It has been proposed that the size of the particles plays a key role in their adhesion and interaction with the biological cells. Nanoparticles of 100 to 200 nm size acquire the best properties for cellular uptake. It is well known that fatty substance and cell uptake can be related with their melting point and degree of carbon chain saturation. Dynasan 114 has a low melting point of 58.63 °C which is further suppressed to 40 °C when converted to nanoparticles. A lower melting could be one of the reasons for preferential uptake of lower melting substances i.e., lipid nanoparticles by the cells.

Cells incubated with STV-DS showed less fluorescence intensity in cell lysate. Around 4% cellular uptake of STV-DS was observed after 120 min. Further increase in incubation time did not lead to any enhancement in drug uptake. It was found that lipid nanoparticles showed very rapid increase in cellular uptake as the time progressed. The higher intensity of dye was obtained within 5 min suggesting that the negatively charged NP bind at cationic sites in the form of a cluster. In addition, the adsorbed nanoparticles on cell surface present a reduced charge density that might have favored adsorption of nanoparticles. NP showed faster uptake up to 12% within few minutes than that of STV-DS. Very high fluorescence intensity (Fig. 3) was obtained for NP after 1 h which is further sustained up to 2 h.

The NP were able to remain in cytoplasm for longer time further crossing the nuclear membrane at the end of 1 h (Lecaroz et al. 2006). The fluorescence photomicrograph shows the formation of nanoparticles clouds around the cell surface. This could be due to a start of diffusion of dye from NP from cell after 1 h. Phase contrast photo micrographs further confirmed the results (Fig. 4).

Phase contrast micrographs also clearly show that the intensity of nanoparticles was highes in nucleus than in cytoplasm. Jayagopal et al. (2008) showed functionalized SLN (fSLN) to interact with endothelial cell monolayers and help in transendothelial transport capabilities.

2.4. MTT cell viability assay

To assess the cytotoxicity of nanocarriers, a MTT assay was performed. Fig. 5. shows the percent viability of cells after incubation with pure drug and lipid nanoparticles of stavudine. At a lower concentration of 0.6 μg/ml high cell viability was observed as compared to STV-DS as well as NP indicating low toxicity at this concentration. The cell viability was found to decrease with increase in concentration of stavudine up to

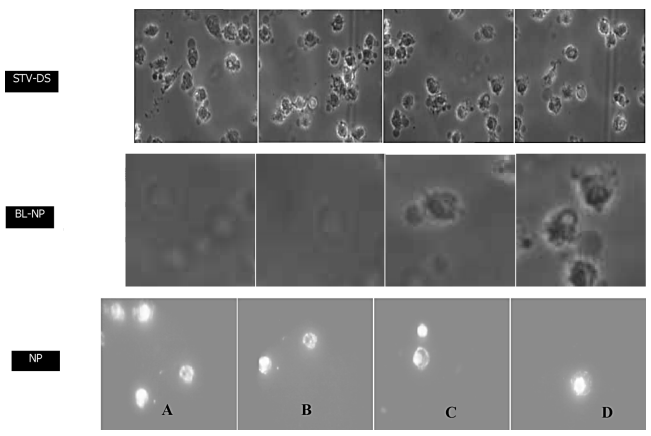

Fig. 4: Phase contrast photomicrographs of primary macrophages incubated with fluorescently labeled nanoparticles A) 10 min B) 30 min c) 60 min and d) 120 min

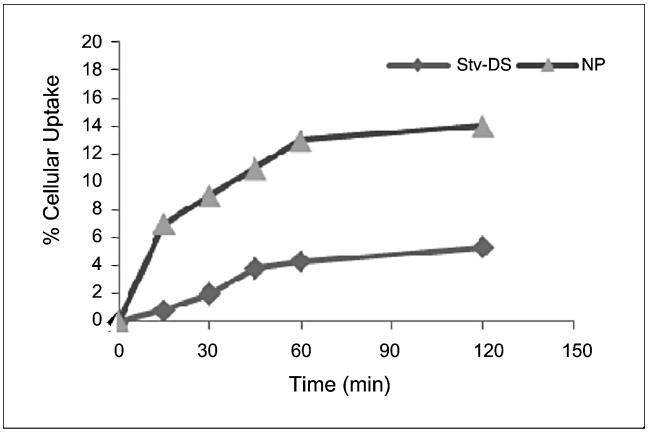

(A)

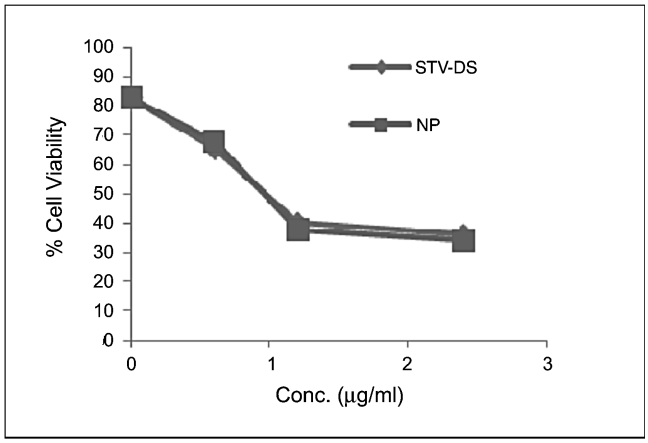

(B)

Fig. 5: Percent phagocytosis of stavudine lipid nanoparticles when incubated with primary macrophages (left) and percent cell viability as determined by MTT assay (right)

1.2 µg/ml. Cytotoxicity of NP was found to comparable to that of STV-DS.

Entrapment of stavudine in lipid nanoparticles or composition of nanoparticles did not show any additional toxicity to cells. The 50% growth inhibition (IC_{50}) value of cell for biocompatible NP was 0.6 µg/ml. Cellular uptake studies have shown a higher uptake of nanoparticles by the macrophages with probable higher drug concentration within the cells (Dou et al. 2006). Even at high concentration within cell cytoplasm the MTT assay confirmed no additional cytotoxicity as compared to pure drug. Nassimi et al. (2009) also obtained low cellular toxicity for prepared SLN. Thus loading of stavudine into nanoparticles did not increase the cytotoxicity of the drug.

2.5. Pharmacokinetics and tissue distribution studies on Stavudine lipid nanoparticles

Radiolabelling with $^{99m}Tco_4^-$ was successfully optimized and it was selected over other radionuclides because of its easy availability, cost effectiveness, low radiation dose and short half-life of about 6 h as compared to 60 days for 125I putting less radiation burden. Chemically, $^{99m}Tco_4^-$ is a non-reactive species and does not label any compound by direct addition. In ^{99m}Tc-labeling of many compounds prior reduction of $^{99m}Tco_4$ (from 7+ state to a lower oxidation state 4+ is required. The technetium used for the study was reduced to its lower valency state using stannous chloride dihydrate. The amount of stannous chloride (reducing agent) used for labelling played an important role in determining labelling efficiency.

STV-DS and NP were directly radiolabelled using $SnCl_2$ as a reducing agent. A high amount of stannous chloride leads to the formation of radiocolloids (reduced/hydrolyzed $^{99m}Tco_4^-$), which is undesirable. On the other less amount of stannous chloride resulted in poor labelling. Optimization of $SnCl_2$ concentration showed poor radiolabelling at 50 µg/ml. The radiolabelling efficiency was increased with increase in $SnCl_2$ concentration. Above 90% radiolabelling was obtained at 1000 µg/ml and 2500 µg/ml $SnCl_2$ concentration. Below 1000 µg/ml STV-DS and NP showed radiolabelling between 85 to 91.66%. Above 1000 µg/ml i.e., at 2500 µg/ml SnCl2 concentration radiolabelling was found to be decrease. At optimized concentration of 1000 µg/ml NP showed excellent stability as compared to STV-DS. Similarly BL-NP showed formation of radiolabelled complex. It was observed that in all formulations 1000 µg/ml of $SnCl_2$ resulted in highest labelling efficiency with low amount of free $^{99m}Tco_4$ (Table 1).

It was observed that at pH 7.01 ± 0.11 the labelling efficiency was highest. Lower and higher values of pH resulted in poor labelling. It was observed that an incubation time below 30 min showed poor radiolabelling and incubation times above 30 min did not further increase the radiolabelling efficiency. Thus maximum radiolabelling was obtained after 30 min incubation. Throughout the whole study optimized incubation time and pH were maintained. Further radiolabelled formulations were subjected to *in vitro* stability tests in PBS (pH 7.4) and plasma. All formulations showed excellent *in vitro* stability of 84–98% stability even after 24 h. NP showed excellent radiolabelling up to 8 h which was slightly decreased to 73.23% after 24 h. In parallel, the stability of the radioactive technetium labelling of the nanoparticles has been controlled in biological medium by incubating the radiolabelled nanoparticles with human plasma at 37 °C indicated that ^{99m}Tc-NP stability was excellent even following a 24 h incubation period. The excellent binding affinity of ^{99m}Tc-NP was challenged showed that low percentages of DTPA does not have much effect on binding affinity but at higher concentration, i.e., 2%, DTPA caused a reduction in labelling by about 8.02–9.87%. This could be due to higher strength and binding affinity of ^{99m}Tc with STV-DS and NP. Approximately 85–88% of the complex remained labelled when subjected to *in-vivo* plasma stability tests. It was observed that STV-DS and NP showed excellent *in-vivo* stability.

After intravenous injection of STV-DS, high blood activity with peak at 5 min was observed (Fig. 6). The count declined sharply thereafter with no blood radioactivity seen at 8 h. This could be due to the very short biological half life of stavudine of 0.9 to

Table 1: Quality control check of radiolabelled ^{99m}Tc-lipid nanoparticle complexes

T (h)	*In-vitro* stability in PBS		*In-vitro* stability in plasma		*In-vivo stability*	
	BL-NP	NP	BL-NP	NP	BL-NP	NP
1	96.5 ± 1.13	95.4 ± 1.10	96.6 ± 1.39	95.1 ± 2.11	94.2 ± 1.55	95.3 ± 1.42
4	92.6 ± 1.55	93.6 ± 2.48	94.9 ± 2.18	91.8 ± 2.15	92.8 ± 1.32	94.6 ± 1.25
8	92.3 ± 2.03	90.5 ± 2.28	92.9 ± 1.15	91.7 ± 1.63	92.2 ± 1.58	93.2 ± 1.32
24	86.1 ± 1.68	87.7 ± 1.39	90.7 ± 2.18	88.4 ± 1.81	90.7 ± 1.60	91.3 ± 1.62

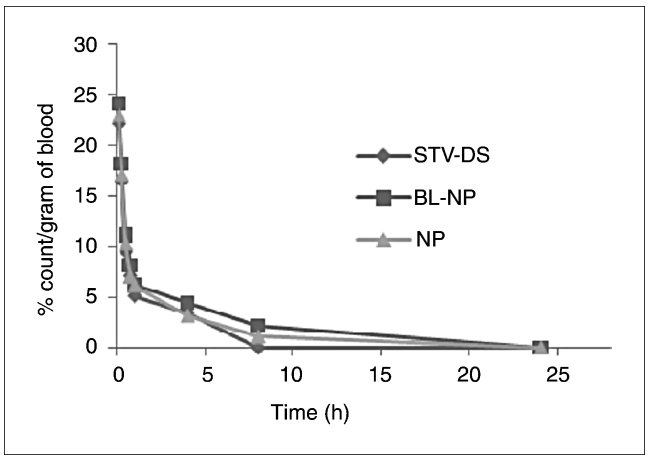

Fig. 6: Comparative blood clearance profile of ^{99m}Tc-STV-DS and NP at different time intervals in rats (n = 3)

1.2 h. In contrast, ^{99m}Tc labelled NP circulated in blood for a longer period of time and blood radioactivity was seen beyond 8 h. Both BL-NP and NP showed prolonged circulation indicating slower clearance of the drug entrapped in nanoparticulate lipid matrix and the appropriate size which permits longer circulation. This is further evident from higher MRT of 3.369 h for NP as compared to 2.055 h for STV-DS. AUC_0^{24} for NP was higher as compared to STV-DS confirming higher bioavailability. The results are in agreement with an earlier report on SLN by Lee et al. (2005).

Gamma imaging after i.v. administration of ^{99m}Tc-labelled STV-DS and NP showed clear distribution in rat. Gammascintigrams obtained are shown in Fig. 7 depicting biodistribution profile at 0.5, 1, 4, 8 and 24 h for STV-DS, BL-NP and NP. It was observed that STV-DS accumulated maximally in the kidney and bladder indicating its rapid excretion with a peak gamma count at 1 h followed by a sharp decline and no radioactivity being observed after 8 h. The kidney and bladder activities in STV-DS group animals at a given time were much higher. Excretion via kidney and urinary bladder was not much prominent in case of NP as compared to STV-DS. The results of the evaluation of NP distribution as obtained by non-invasive planar scintigraphic imaging in rats showed that they are rapidly cleared from blood and reached to RES organs (liver and spleen) leading to higher radioactivity ($p < 0.05$) within 30 min and were able to retain in these organs for a prolonged period. This may be attributed to the natural passive uptake of the colloidal carriers by liver cells (Desormeaux and Bergeron 2005).

.

The developed nanoparticulate formulation contains a large fraction of spherical populations small enough to escape the space of blood vessel and tissue and reaching hepatocytes or macrophages. However, even at an early stage of scanning and

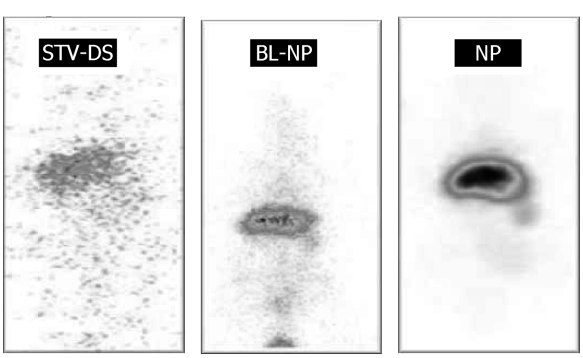

Fig. 7: Gammascintigraphs depicting distribution of radioactivity at 4 h.

Table 2: Enhancement of gamma count obtained by NP over STV-DS

Time (h)	Enhancement in gamma count	
	Blood	Spleen
1	1.19	2.59
4	0.91	6.86
8	1.11	8.30
24	–	1.12

even 8 h after injection the liver is clearly distinguishable. Therefore BL-NP and NP showed comparable accumulation in RES organs. The localization of formulations was more prominent at 4 h and 8 h.

After 24 h, the STV-DS were completely excreted from body whereas BL-NP and NP were able to retain in smaller amounts in RES organs as compared to STV-DS. We were unable to outline the kidneys suggesting a slow excretion rate of NP and the bladder image was also unresolved. Encapsulation of the stavudine into the lipid core reduced its excretion through kidney and allowed more deposition in the liver and spleen as shown in gammascintigrams. The liver and spleen represented the main sites of Technetium (Tc) labelled NP uptake as early as 30 min post injection and tracer activity remained stable until 24 h after injection (Daemen 1992). The data indicated that lipid nanoparticles were rapidly cleared from the blood compartment to localize to the mononuclear phagocyte system, particularly to liver and spleen macrophages after injection via the intravenous route in rats. It was clear from scintigrams that the whole body imaging did not show any ^{99m}Tc accumulation in the brain. None of the formulations was able to cross blood brain barrier.

The use of a stable technetium labelled NP allowed for the first time an extended follow up of the biodistribution in rat. After studying the distribution pattern of NP by gamma imaging it was important to know its concentration in each tissue. During the *in-vivo* studies animals did not show any visible symptoms of toxicity related to the injection of the radiolabelled NP and this should be highlighted since this is the first report on stavudine lipid nanoparticles for intravenous administration.

Any drug or formulation when injected intravenously first goes to heart, from where it gets distributed to other organs/tissues via arterial blood. During this process there is ample possibility of the injected drug or formulations being uptaken by the cardiac muscles. So it is important to determine the drug retention in circulatory organ.

Cardiac retention of all the formulations was determined by measuring the gamma count in the heart. A relatively high level of activity was observed initially in the lung/heart region before the nanoparticles were cleared by the RES. Highest AUC_0^{24} of 62.88 counts·h/g was obtained for NP as compared with STV-DS (22.336 counts·h/g) in heart. MRT of drug loaded NP was found to be three times higher than that of STV-DS (Fig. 9). NP showed higher levels of gamma count maintaining up to 24 h as compared to STV-DS in lungs. Drug loaded nanoparticles showed 1.46 fold enhancement in gamma count as compared to STV-DS (Table 2). Stavudine nanoparticles showed higher AUC_0^{24} of 154.955 counts·h/g as compared to STV-DS (122.505 counts·h/g).

NP showed 1.03 fold increase in gamma count compared with pure drug with slight increase in AUC_0^{24} (335.55 counts·h/g) than that of STV-DS (301.945 counts·h/g) in liver but STV-DS showed higher MRT of 10.817 h as compared to NP. Drug loaded lipid nanoparticles showed 8.30 fold increase in gamma count over STV-DS in spleen. High spleenic uptake with

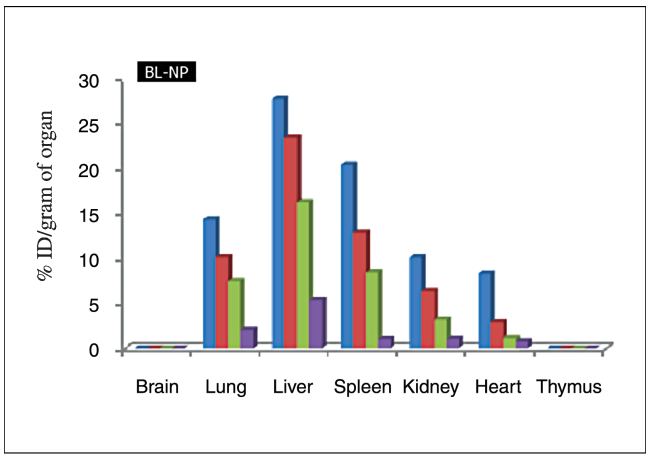

(A)

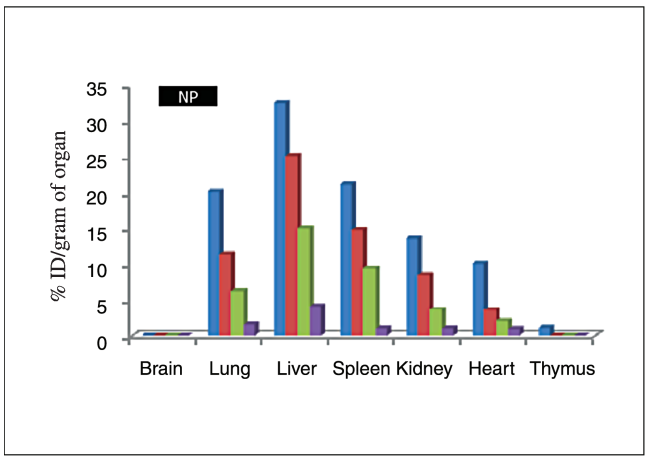

(B)

Fig. 8: Radioactivity of stavudine lipid nanoparticles in different organs for various experimental group

$AUC_0{}^{24}$ of 196.605 counts·h/g for NP which was observed to be much higher as compared to that of 35.133 counts·h/g obtained for STV-DS. The mean residence time was prolonged i.e., almost two times higher than STV-DS. Patil et al. (2008) showed similar results and evaluated the role of lipid matrix. It was found that STV-DS, BL-NP and NP were not able to cross the blood brain barrier and thymus which also serves as important organ in HIV latency.

The hepato-splenic distribution was largely dependent on the histological structure of vascular endothelium of these tissues and physicochemical property of nanoparticles. As the developed lipid nanoparticulate formulations has the tendency to accumulate in liver and spleen so their elimination half-life was longer.

3. Experimental

3.1. Materials

Stavudine was received as generous gift sample from Alkem Laboratories, Mumbai, India. Dynasan 114 (Trimyristin) and Solutol HS 15 were obtained as gift sample from Sasol GmbH, Plurol® Oleique CC 497 received as gift sample from Gattefossé, France. Poloxamer 188 (BASF Inc.) and Tween 80 (S. D. Fine chemicals) were obtained. RPMI (Roswell Park Memorial Institute) medium, fetal calf serum (FCS), dimethyl sulfoxide (DMSO), yellow MTT (3- (4, 5-dimethyl-thiazol-2-yl)-2, 5-diphenyl-tetrazolium bromide, tetrazole), MTT solution (prepared by dissolving 5 mg of MTT + 1 ml of medium without phenol red), DMEM, acid propanol, diethylene triamine penta acetic acid (DTPA), acetone AR grade, sodium chloride (NaCl) and stannous chloride ($SnCl_2$) were purchased from S.D. Fine Chemicals, Mumbai.

3.2. Preparation of solid lipid nanoparticles (NP)

Stavudine nanoparticles were prepared in an APV 2000 lab model high pressure homogenizer. In brief, the drug was dissolved in 2% w/v melted lipid containing hydrophobic surfactants (3% w/w) and slowly dispersed in aqueous surfactant solution (0.5%) of the same temperature to form a pre-emulsion. The formed microparticles were then homogenized. The homogenization parameters were then optimized keeping number of homogenization cycles constant and its effect on the mean particle size was studied.

3.3. Characterization of lipid nanoparticles

3.3.1. Organoleptic properties

The homogenized batches of lipid nanoparticles were evaluated for various physicochemical properties such as color, odor, pH, physical instability. The stavudine lipid nanoparticles that were stable after 24 h were subjected to centrifugation at various speeds from 2000 to 20,000 rpm for 10 min and any incidences of creaming, cracking or phase separation were recorded.

3.3.2. Drug content

Total drug content of nanoparticles was analyzed using liquid-liquid extraction using chloroform and phosphate buffer pH 7.2. The clear aqueous portions were analyzed spectrophotometrically at 265 nm. The amount of drug was calculated from the standard curve equation.

3.3.3. Zeta potential (electrokinetic potential)

Lipid nanoparticles of stavudine were diluted in miliQ water and zeta potential (n = 10) was determined using Brookhaven Zeta Pals, BI-Zetaman, Ver. 1(Brookhaven Instruments Corp., NY, USA).

3.3.4. Particle size determination

Photon correlation spectroscopy (PCS) technique is suitable for application to particles ranging in size 3 to 3000 nm. Mean particle size and particle size distribution and polydispersity index (PI) of developed lipid nanoparticles was determined using a N5 Beckman submicron particle size analyzer at a fixed angle of 90° at 20 °C in double distilled water as dispersant.

Laser diffraction (LD) was performed using a Mastersizer 2000 (Malvern Instruments, UK). The instrument was operated with the Hydro S sample dispersion. LD yields volume weighted diameters. The d(v)50% represents the size where 50% of the particles are below the given size. D(v)95% and d(v)99% are sensitive parameters to quantify potential larger sized particles present.

3.3.5. Transmission Electron Microscopy

TEM images of drug loaded lipid nanoparticles were acquired using a transmission electron microscope, Philips CM, operating voltage 20–200 Kv model with Resolution 2.4 Aº. Sufficient quantity of lipid nanoparticles was placed on coated copper grids and allowed to settle for 3 to 5 min in a petri plate. The excess of formulation was removed by tilting the petri dish and dried under an UV lamp. Dried copper grids were stained with 1% uranyl acetate solution and loaded on the transmission electron microscope and area of interest was scanned for observation of nanoparticles and images were obtained.

3.3.6. DSC measurements

The stavudine NP were studied for their thermal behavior using differential scanning calorimetry Mettler DSC 821e (Gieen, Germany). Accurately weighed samples (1–4 mg) were placed in non hermetically sealed standard aluminum pans. An empty aluminum pan served as a reference. Heating scans for each sample were performed from 25 to 200 °C at 10 °C/min. The heating rate was 10 K/min with a nitrogen purge of 80 ml/min. The DSC parameters including the melting point and melting enthalpy were evaluated using the STARe Software (Mettler Toledo, Switzerland).

3.4. Cellular uptake studies

3.4.1. Lavage of macrophages

The primary peritoneal macrophages were harvested from male Wister rats by injecting 10 ml thioglycollate medium intraperitoneally to Wister rats (180–220 g) (Huang et al. 2005). Three days later the animals were deeply anesthetized by ether and 10 ml of freshly prepared HBSS were injected into the peritoneal cavity. After 3 min gentle massage the abdomen was Haub's buffered salt solution (HBSS) opened and HBSS was recovered. The lavaged cell suspension was then centrifuged at 1300 rpm at 4 °C, and the pellet was resuspended in HBSS. The cell preparation was enriched in macrophages by the following method.

3.4.2. Monolayer formation and uptake

Peritoneal macrophage cells were cultured in sterilized culture plates containing glass cover slips at a seeding density of 1×10^6 cells/ml. RPMI 1640 medium supplemented with 10% fetal bovine serum was added to each well and incubated at $37 \pm 2\,^{\circ}$C at 5% CO2 for 24 hours to form a confluent monolayer. After three hours of incubation macrophages were washed and rinsed twice with HBSS to remove the non-adherent cells. Monolayer formation was checked under a light microscope. After equilibration, cellular uptake of nanoparticles was initiated by exchanging the transport medium with freshly prepared fluorescent nanoparticles of stavudine at $37 \pm 2\,^{\circ}$C. The Rhodamine 123 was used as fluorescence marker and was entrapped in solid lipid vesicles instead of drug. In each culture well, 500 µl of pure drug (STV-DS) or nanoparticles (NP) at 750 µg/ml stavudine per ml of formulation was added. Plain Rhodamine solution was used as blank. The plates were incubated in a controlled environment at a temperature of $37\,^{\circ} \pm 2\,^{\circ}$C for a period of 0, 15, 30, 45, 60 and 120 min.

3.4.3. Qualitative determination

Fluorescence microscopy was performed to study the qualitative uptake of prepared nanoparticles in comparison to plain dye. After treatment, at specific interval cells were washed with PBS thrice and the cover slip was mounted on a clean sterilized glass slide and fixed. The slide was immediately observed under Olympus Fluorescence microscope and photomicrographs were captured at different time points and observations were recorded.

3.4.4. Quantitative determination

At specified times intervals, the phagocytosis was terminated by immersing the plate in an ice bath. The cell monolayer were washed three times using ice cold PBS (pH 7.4) to remove non-adherent particles, The cells were separated from the medium by centrifugation at 2000 rpm for 15 min (Sorvall Biofuge Primo R centrifuge, Thermo Electron Corporation, India) and the supernatant was collected. The cells were further lysed using hypotonic saline and centrifuged again at 10,000 rpm. The fluorescence associated with the nanoparticles harvested cells and supernatant was determined using fluorimetry at λ_{ex} 485 nm, λ_{em} 529 nm. The percent cellular uptake was calculated using the following formula,

$$\text{Uptake efficiency}\,(\%) = (W_{sample}/W_{total}) \times 100\% \quad (1)$$

Where W_{sample} is the amount of fluorescence associated with macrophage cells, and W_{total} is the amount of fluorescence present in the feed nanoparticle. The experiment was run in triplicate for each formulation and results were expressed as the mean ± SD.

3.5. MTT cell viability assay

The cell viability was determined in murine macrophages J774.A12 (National Centre for Cell Sciences, Pune, India) using 3-(4,5-dimethylthiazol-2-yl)-2,5-diphenyl-tetrazolium bromide i.e., MTT. The murine macrophages were seeded in a density of 1×10^5 in 96 flat well bottom culture plates containing 200 µl of DMEM and incubated overnight. The cells were counted using the trypan blue method in a Neubauer chamber and suspended in RPMI with 10% FCS, 100 U of penicillin/ml and 100 µg of streptomycin/ml and incubated at $37 \pm 2\,^{\circ}$C (Forma Scientific Inc., Marjetta, OH, USA). After overnight incubation, the cells were washed thrice with DMEM and suspended in 80 µl of fresh DMEM. In each plate, 20 µl of the drug solution or formulation was added. After 24 h treatment, 10 µl of 2 mg/ml MTT solution was added to culture plates and incubated for 6 h at $37 \pm 2\,^{\circ}$C. After 6 h, the MTT reaction was terminated by addition of acid propanol (1 M Hcl: isopropanol in 1:24 ratio). At the end of the incubation period, the medium was removed and the converted dye was solubilised in acidic propanol. Absorbance of converted dye was measured spectrophotometrically at 570 nm and viability expressed in percentage compared to control and standard solution.
The percent cytotoxicity was calculated for all the experiments and reported as mean of three determinations

$$\%\,\text{Cytotoxicity} = \frac{(100 - \text{Optical density}_{PBS})}{(\text{Optical density}_{PBS}) - (\text{Optical density}_{TEST})} \times 100 \quad (2)$$

The experiment was run in triplicate for each formulation and results were expressed as the mean ± SD.

3.6. Radiolabelling of stavudine lipid nanoparticles

Gamma scintigraphy is a widely use technique for assessing the biodistribution pattern of colloidal carriers (Banerjee et al. 2002). ^{99m}Tc was obtained by separation from the parent molybdenum (^{99m}Mo) by alumina column solvent extraction technetium generator. Parent ^{99m}MO (50 mCi activity) was procured from Board of Radiation and Isotope Technology (B.R.I.T.), Mumbai.
The pure drug solution, blank and drug loaded lipid nanoparticles of stavudine were labelled with ^{99m}Tc by a direct labelling method using $SnCl_2$ as a reducing agent (Richardson et al. 1977). Briefly, 1 ml of ^{99m}Tc (1.2 mCi) was mixed with 0.1 ml of $SnCl_2$ solution (1 mg/ml) in 0.1 N HCL to reduce the technetium. The pH of solution was adjusted to 6.9–7.1 using Tris buffer. To this mixture, either 1 ml of STV-DS (1.5 mg/ml) or NP (lipid concentration 20 mg/ml) was added and incubated for 30 min at room temperature. The quality control i.e., percent labelling efficiency and stability of labelled complexes was performed. The labelling efficiency was determined by ascending thin layer chromatography (TLC) using silica gel coated sheets. TLC was performed using acetone or 0.9% saline as mobile phase. Approximately 2 to 3 µl of the radiolabelled complex was applied at a point 1 cm from one end of an TLC strip. The strip was developed in acetone or 0.9% saline and the solvent front was allowed to reach 8 cm for the point of application. The strip was cut into two portions i.e., upper two thirds and lower third and the radioactivity in each segment was determined in a well type gamma ray counter (Gamma-ray scintillation counter, Type CRS 23C, Electronics Corporation of India Ltd., Mumbai, India).

$$\text{Radiolabelling efficiency}(\%) = (LE/(UE + LE)) \times 100 \quad (3)$$

where
LE: Count at Lower (1/3) End; UE Count at Upper (2/3) End
Optimization of Radiolabelling conditions:
pH: The complex was incubated at different pH values of 5, 6, 7, and 8 at room temperature. The labelling efficiency was determined by TLC.
Time of incubation: The complex was incubated for different time periods viz., 0, 5, 15, 30 and 45 min at room temperature. The labelling efficiency was estimated.
$SnCl_2$ concentration: The complex was prepared using different concentration of $SnCl_2$ viz., 50, 250, 500, 1000 and 2500 µg/ml incubated with formulations at room temperature and the labelling efficiency was determined.
Stability studies of the nanocarriers-^{99m}Tc complex. In vitro stability in PBS: For the determination of *in vitro* stability of all ^{99m}Tc-NP complex, 100 µl of the labelled formulation was mixed with 2.0 ml of PBS (pH 7.4) and incubated at room temperature and change in labelling efficiency was monitored over a period of 24 h by TLC in acetone or 0.9% saline.
In vitro stability in plasma: The radiolabelled pure drug solution, blank and drug loaded lipid nanoparticles (1.2 mCi) were mixed and incubated in 1.9 ml human plasma at $37 \pm 1\,^{\circ}$C. TLC was performed time to time and checked for dissociation of free technetium from complex.
Transchelation of complexes with DTPA: The stability and bonding strength of complexation of ^{99m}Tc with drug and stavudine lipid nanoparticles was challenged against various concentrations (0.05%, 0.5%, 1% and 2%) of diethylene triamine penta acetic acid (DTPA) and incubated for 2 h at $37 \pm 2\,^{\circ}$C. The effect of DTPA on labelling efficiency was measured on ITLC using acetone as the mobile phase which allowed the separation of free pertechnetate and DTPA-complex (Rf = 0.8–1.0) from the ^{99m}Tc labelled drug and lipid nanoparticles, which remained at the point of application.
In vivo stability of the labelled complexes: Animals were injected 1.2 mCi of ^{99m}Tc labelled formulations through the tail vein. The blood was withdrawn through the retro-orbital vein at different time intervals and spotted on the TLC strips. The TLC was carried out to estimate the separation of free ^{99m}Tc/degradation of complex.

3.7. Instrument details

In present the study, all scintigraphy imaging was performed under "Millennium MPS Acquisition System, Multi Purpose Single Head, square detector gamma camera" (General Electrical, U.S.A) and processed by eNTEGRA work station. Genieacq acquisition computer with data acquisition software programs were suitable for the acquisition of images in static and dynamic modes.

3.8. Pharmacokinetic and biodistribution studies

In-vivo evaluation of the developed formulations was carried out in three parts a) Pharmacokinetic studies b) Gamma imaging and c) Tissue distribution studies. Rats were anesthetized with an intraperitoneal injection of ~30 µL of 1:1 mixture of ketamine (10% w/v or 75 mg/kg) and xylazine

(2% w/v or 15 mg/kg). The animals were divided into the following groups containing three rats each. All the rats were weighed and a single dose of 2.7 mg/kg radiolabelled (1.2 mCi) STV-DS and NP was administered by intravenous (via tail vein) route by using BDTM Micro-Fin syringe, insulin type (29 G). All animal experiments were approved by Institutional ethical committee of Bombay Veterinary College, Mumbai, India and conducted under supervision of expert veterinarian.

3.8.1. Blood clearance

The blood kinetics of radiolabelled stavudine drug solution (STV-DS), blank nanoparticles (BL-NP) and drug loaded nanoparticles (NP) were studied by injecting 1.2 mCi of radiolabelled complex in animal. After administration, blood was collected from retro-orbital puncture using a fine glass capillary into a small glass test tube containing 0.3% sodium citrate solution at stipulated time intervals of 5, 15, 30, 45 min, 1, 4, 8 and 24 h. Radioactivity was measured in the whole blood per gram of sample using well-type gamma scintillation counter (Gosh et al. 2006).

3.8.2. Gamma scintigraphy imaging

Animals were administered 1.2 mCi of radiolabelled formulations through the tail vein. Noninvasive whole body planar imaging was performed using a Millennium MPS Gamma camera system auto tuned to detect the 140 keV radiation of ^{99m}Tc. After specified time intervals of 0.5, 1, 2, 4, 8 and 24 h the rats were fixed on board and imaging was performed using gamma camera.

3.8.3. Biodistribution studies by post-mortem assessment

Rats were anesthetized and bolus intravenous injections of freshly prepared radiolabelled STV-DS, BL-NP and NP (1.2 mCi) were given via the tail vein. After administration at a specified time interval of 1, 4, 8 and 24 h animals were humanly sacrificed using inhalation of a high amount of anesthetic ether. The rats were dissected and major tissues like brain, lung, liver, kidney, spleen, heart and thymus were removed and washed with Ringer's solution to remove any adherent debris and dried using tissue paper. The organs were weighed and triturated to form a homogenate. Radioactivity corresponding to per gram of organ was measured using a well-type gamma scintillation counter.

3.9. Data processing

To calculate the total theoretical activity at different time points in organs decay factor was taken into account and then expressed as a percentage of this value. The results were expressed as after decay correction, the organ activity of the nanoparticles was expressed as percentage of the injected dose per gram of weight (% ID/g). Pharmacokinetic parameters like C_{max}, T_{max}, area under zero-moment curve (AUC), area under first-moment curve (AUMC), mean residence time (MRT) for stavudine nanoparticles were calculated using GraphPad Prism software (version 4.03, USA); < 0.05 was considered as statistically significant difference. All the results are expressed as the mean $\pm$ SD and statistical analysis was assessed using student's t-test at $p < 0.05$ as the minimum level of significance.

Acknowledgements: The authors would like to thank AICTE (All India Council of Technical Education) for financial support. Bombay Veterinary college for providing facility for carrying out Gammascintigraphy studies and PERD Centre for cellular uptake studies.

References

Al-Haj N, Rasedee A (2009) Solid lipid nanoparticles preparation and characterization. Int J Pharmacol 5: 90–93.

Amiji MM, Vyas TK, Shah LK (2006) Role of nanotechnology in HIV/AIDS treatment: potential to overcome the viral reservoir challenge. Discov Med 6: 157–162.

Banerjee T, Mitra S, Kumar Singh A, Kumar Sharma R, Maitra A (2002) Preparation, characterization and biodistribution of ultrafine chitosan nanoparticles. Int J Pharm 243: 93–105.

Daemen T (1992) Activation of Kupffer cell tumoricidal activity by immunomodulators encapsulated in liposomes. Res Immunol 143: 211–214.

Desormeaux A, Bergeron MG (2005) Lymphoid tissue targeting of anti-HIV drugs using liposomes. Methods Enzymol 391: 330–351.

Dou H, Destache CJ, Morehead JR, Mosley RL, Boska MD, Kingsley J, Gorantla S, Poluektova L, Nelson JA, Chaubal M, Werling J, Kipp J, Rabinow BE, Gendelman HE (2006) Development of a macrophage-based nanoparticle platform for antiretroviral drug delivery. Blood 108: 2827–2835.

Dou H, Morehead J, Destache CJ, Kingsley JD, Shlyakhtenko L, Zhou Y, Chaubal M, Werling J, Kipp J, Rabinow BE, Gendelman HE (2007) Laboratory investigations for the morphologic, pharmacokinetic, and anti-retroviral properties of indinavir nanoparticles in human monocyte-derived macrophages. Virology 358: 148–158.

Escobar Y, Venturelli CR, Escobar-Islas E, Hoyo-Vadillo C (2003) Pharmacokinetics of stavudine by oral administration to healthy Mexican volunteers. Proc West Pharmacol Soc 46: 109–110.

Ghosh PK, Majithiya RJ, Umrethia ML, Murthy RS (2006) Design and development of microemulsion drug delivery system of acyclovir for improvement of oral bioavailability. AAPS PharmSciTech 7: 77.

Gordon R, Bjorklund NK, Smith RJ, Blyden ER (2009) Halting HIV/AIDS with avatars and havatars: a virtual world approach to modelling epidemics. BMC Public Health 9 Suppl 1: S13.

Guimaraes NN, de Andrade HH, Lehmann M, Dihl RR, Cunha KS (2010) The genetic toxicity effects of lamivudine and stavudine antiretroviral agents. Expert Opin Drug Saf.

Hou D, Xie C, Huang K, Zhu C (2003) The production and characteristics of solid lipid nanoparticles (SLNs). Biomaterials 24: 1781–1785.

Huang M, Wu W, Qian J, Wan DJ, Wei XL, Zhu JH (2005) Body distribution and in situ evading of phagocytic uptake by macrophages of long-circulating poly (ethylene glycol) cyanoacrylate-co-n-hexadecyl cyanoacrylate nanoparticles. Acta Pharmacol Sin 26: 1512–1518.

Jain SK, Gupta Y, Jain A, Saxena AR, Khare P (2008) Mannosylated gelatin nanoparticles bearing an anti-HIV drug didanosine for site-specific delivery. Nanomedicine 4: 41–48.

Jayagopal A, Sussman EM, Shastri VP (2008) Functionalized solid lipid nanoparticles for transendothelial delivery. IEEE Trans Nanobioscience 7: 28–34.

Kuo YC (2005) Loading efficiency of stavudine on polybutylcyanoacrylate and methylmethacrylate-sulfopropylmethacrylate copolymer nanoparticles. Int J Pharm 290: 161–172.

Lanao JM, Briones E, Colino CI (2007) Recent advances in delivery systems for anti-HIV1 therapy. J Drug Target 15: 21–36.

Lecaroz C, Blanco-Prieto MJ, Burrell MA, Gamazo C (2006) Intracellular killing of Brucella melitensis in human macrophages with microsphere-encapsulated gentamicin. J Antimicrob Chemother 58: 549–556.

Lee CM, Choi Y, Huh EJ, Lee KY, Song HC, Sun MJ, Jeong HJ, Cho CS, Bom HS (2005) Polyethylene glycol (PEG) modified ^{99m}Tc-HMPAO-liposome for improving blood circulation and biodistribution: the effect of the extent of PEGylation. Cancer Biother Radiopharm 20: 620–628.

Löbenberg R, Araujo L, von Briesen H, Rodgers E, Kreuter J (1998) Body distribution of azidothymidine bound to hexyl-cyanoacrylate nanoparticles after i.v. injection to rats. J Control Release 50: 21–30.

Mehnert W, Mader K (2001) Solid lipid nanoparticles: production, characterization and applications. Adv Drug Deliv Rev 47: 165–196.

Nassimi M, Schleh C, Lauenstein HD, Hussein R, Lubbers K, Pohlmann G, Switalla S, Sewald K, Muller M, Krug N, Muller-Goymann CC, Braun A (2009) Low cytotoxicity of solid lipid nanoparticles in *in vitro* and *ex vivo* lung models. Inhal Toxicol 21 Suppl 1: 104–109.

Patil RR, Gaikwad RV, Samad A, Devarajan PV (2008) Role of Lipids in Enhancing Splenic Uptake of Polymer-Lipid (LIPOMER) Nanoparticles Journal of Biomedical Nanotechnology 4: 359–366.

Richardson VJ., Jeyasingh K., F. JR (1977) Properties of [^{99m}Tc] technetium-labeled liposomes in normal and tumour-bearing rats. Biochem Soc Trans 5: 190–229.

Schafer V, von Briesen H, Andreesen R, Steffan AM, Royer C, Troster S, Kreuter J, Rubsamen-Waigmann H (1992) Phagocytosis of nanoparticles by human immunodeficiency virus (HIV)-infected macrophages: a possibility for antiviral drug targeting. Pharm Res 9: 541–546.

Sosnik A, Chiappetta DA, Carcaboso AM (2009) Drug delivery systems in HIV pharmacotherapy: what has been done and the challenges standing ahead. J Control Release 138: 2–15.

Vyas SP, Subhedar R, Jain S (2006a) Development and characterization of emulsomes for sustained and targeted delivery of an antiviral agent to liver. J Pharm Pharmacol 58: 321–326.

Vyas TK, Shah L, Amiji MM (2006b) Nanoparticulate drug carriers for delivery of HIV/AIDS therapy to viral reservoir sites. Expert Opin Drug Deliv 3: 613–628.

zur Muhlen A, Schwarz C, Mehnert W (1998) Solid lipid nanoparticles (SLN) for controlled drug delivery–drug release and release mechanism. Eur J Pharm Biopharm 45: 149–155.